

Structure-Based Drug Design of Diphenyl α -Aminoalkylphosphonates as Prostate-Specific Antigen Antagonists

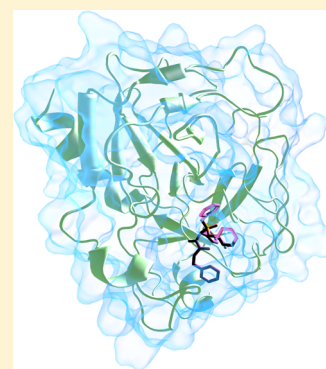
Arben Kojtari,[†] Vishal Shah,[†] Jacob S. Babinec,[†] Catherine Yang,[‡] and Hai-Feng Ji^{*,†}

[†]Department of Chemistry, Drexel University, Philadelphia, Pennsylvania 19104, United States

[‡]Department of Chemistry and Biochemistry, Rowan University, Glassboro, New Jersey 08028, United States

Supporting Information

ABSTRACT: Here, we describe the mechanism of diphenyl α -aminoalkylphosphonate ester derivatives as potent inhibitors of prostate-specific antigen (PSA), a likely protease responsible for the advancement of prostate tumor progression. The AutoDock 4.2 molecular docking suite was utilized to model covalent and noncovalent binding of this class of inhibitors to predict crystallographic poses and compare experimental IC₅₀ dose-response curves and in silico potencies for providing future more specific rational drug design. The new lead compound R/S-diphenyl[N-benzyloxycarbonylamino(4-carbamoylphenyl)methyl]phosphonate is being reported in this study as a potent inhibitor of PSA activity (IC₅₀ = 250 nM; AutoDock Score = -8.29/-9.14 kJ·mol⁻¹ for R/S). Molecular dynamics (MD) simulations using GROMACS 4.6.5 was used to obtain trajectories of the top ligand and validate key interactions in the binding complex. A hydrogen-bonding map was used to confirm interactions between the lead compound and residues THR₁₉₀, SER₂₁₇, and SER₂₂₇ in the P1 pocket. The modeling study introduces novel aminoalkylphosphonates as a potential drug candidate for targeting PSA by optimizing P1 binding affinities.



1. INTRODUCTION

Prostate cancer (PCa) is one of the most prevalent cancers diagnosed in adult males. The American Cancer Society estimated that in 2014, over 233 000 new cases of PCa would be diagnosed, and 29 480 deaths would occur due to this disease.¹ Prostate cancer may cause pain, difficulty urinating, erectile dysfunction, and other symptoms but can also metastasize to other tissues within the body.

Chemotherapy has been widely used for PCa treatments. Recent studies have focused on chemotherapy-induced apoptosis of tumor cells to inhibit tumor cell growth and promote cell death. Two important molecular targets for prostate cancer treatment include prostate tissue concentration of secreted growth factors, such as transforming growth factor type-P (TGF-P) and prostate-specific antigen (PSA). TGF-P regulates cell growth, differentiation, and development of a variety of functions. Another target is PSA, a serine protease,² which is known as human glandular kallikrein-related peptidase-3 (KLK3). It is a chymotrypsin-like serine protease secreted from epithelial prostate tissue, where it is highly localized.³ PSA has been found to control the growth of cancer metastasis and proliferation. Regulated by an androgen receptor-mediated transcription pathway, the primary role of PSA biologically is the liquefaction of semen via proteolysis of coagulating proteins fibronectin and semenogelin within the matrix.^{4,5} However, with elevated PSA levels, the protease has been shown to cleave insulin-like growth factor binding protein-3 (IGFBP-3),¹⁷ a modulator of mitogenic proteins insulin-like growth factors (IGF) I and II. It has been demonstrated that the involvement of PSA with the IGF molecular system leads to the progression

of prostate cancer,⁶ which can in turn metastasize into the patient's lymph nodes and bone, causing osteoblastic lesions via PSA-activation of latent transforming growth factor type-beta (TGF- β),⁷ and proteolysis of IGFBP-5.⁸

Although therapies targeting the androgen receptor, an upstream regulator of PSA, have been effective in treating prostate cancer,⁹ the disease state sometimes progresses and results in castrate-resistant prostate cancer.¹⁰ Alternative therapies should be pursued for prostate cancer treatment, especially in the scenario where androgen deprivation fails.

There have been numerous compounds that have been published tailored to act as either PSA substrates or antagonists, such as peptides,¹¹ aldehydes and boronic acids,¹² as well as β -lactam compounds.¹³ However, some drawbacks of these inhibitors include long synthetic routes and moderate potency. It is important to broaden the spectrum of PSA antagonists to diversify the chemical library suitable for treating PCa. To accomplish this, structure-based drug design concepts were used to tailor a class of ligands to the local chemical environment of the PSA binding cavity. Molecular docking, in conjunction with dynamics simulations, have frequently been used to accomplish these tasks for numerous biological targets. Not only can ligand libraries be searched via virtual screening (VS) in docking suites, stability of binding complexes and dynamic residue interactions can be probed using MD simulations.

Received: June 24, 2014

Published: September 4, 2014

Here, we report the synthesis, mechanistic-based binding, and dose-dependent inhibition of the PSA enzyme using α -aminoalkylphosphonates. The facile synthesis was published by Oleksyszyn and co-workers which utilizes a one-pot synthesis to produce diphenyl α -aminoalkylphosphonates using an aldehyde, amine, and a trialkylphosphite.¹⁴ The reaction, known as the Kabachnik–Fields reaction,^{15,16} can be completed with modest yields and facile purification of products via crystallizations. This class of irreversible inhibitors have been studied previously for a variety of biological targets, most of which are serine proteases.^{17–20} These compounds and their derivatives have not been exploited for targeting PSA, with the exception of a few derivatives published recently by Yang and co-workers.²¹ The lack of extensive application of α -aminoalkylphosphonates as PSA antagonists are particularly appealing to expand the inhibitory potential toward the target.

In this work, we have found a new lead compound as a PSA inhibitor by targeting the P1 pocket of the protein through molecular modeling AutoDock 4.2 program, where the P1 site displays binding specificity to the R-group of the amino acid mimic. The P1 pocket of PSA contains the residues SER₂₁₇, SER₂₂₇, and THR₁₉₀ which display affinity for amino acid side chains for proteolytic activity.²² To elucidate S1/P1 specificity in the PSA binding site, we modeled and synthesized analogs of diphenyl [N-(benzyloxycarbonylaminophenylmethyl]phosphonate compounds (Figure 1). These compounds

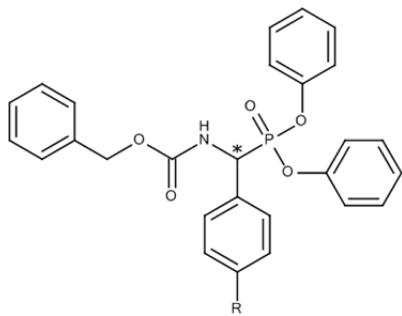


Figure 1. General structure of diphenyl [N-(benzyloxycarbonylaminophenylmethyl]phosphonate analogs synthesized, with 13 varying R-groups. The asterisk indicates the stereocenter.

mimic phenylglycine, which have shown inhibition of a variety of serine proteases and can be tuned synthetically to be site-specific for the P1 pocket of the protein.

2. EXPERIMENTAL SECTION

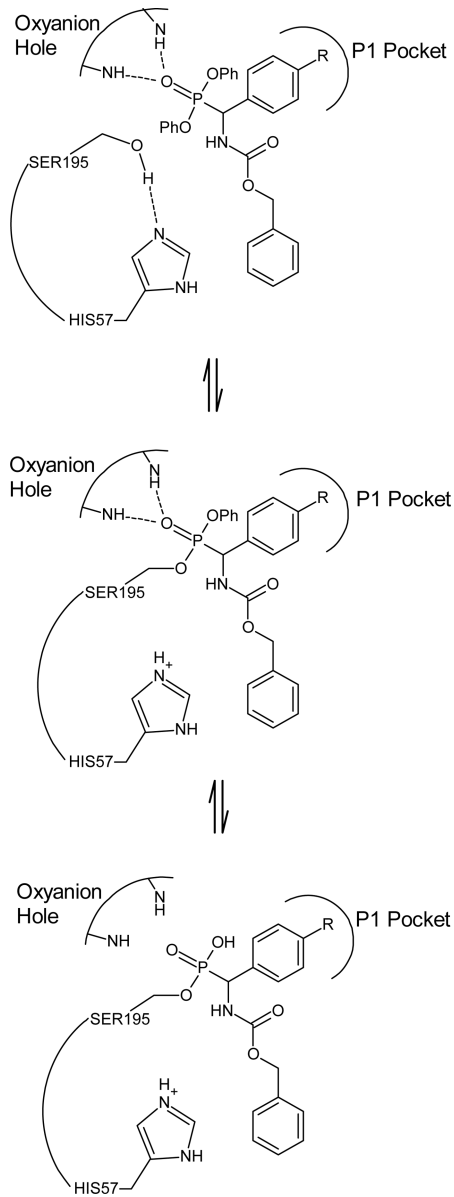
2.1. Ligand Docking Experiments. AutoDock 4.2 uses an empirical force field calculation using two Lennard-Jones potentials to calculate pairwise potentials for the van der Waals and hydrogen-bonding terms, as well as a Coulombic electrostatic and entropic potential parameters. The AutoDock scoring function was parametrized from 30 protein–ligand complexes and their binding constants, majority of which are in the protease class of proteins.²³ Because of the protein-inhibitor complexes chosen in the training set and flexibility of the software, AutoDock 4.2 is a suitable choice for our docking experiments. Specifically, potential binding conformations and free energies were determined *in silico* for the selected α -aminoalkylphosphonates. The scoring function parameters used here omitted internal electrostatics in the calculation, an option allowable in the AutoDock suite. A detailed description of the AutoDock scoring function is described by Morris et al.²⁴

Molecular docking experiments of α -aminoalkylphosphonate inhibitors with PSA were conducted using the software AutoDock 4.2 with AutoDock Tools.²⁵ Ligand files were prepared using HyperChem and minimized with AMBER force field. The three-dimensional structure of human PSA was retrieved from the Protein Data Bank (PDB ID: 2ZCK). Receptor file was prepared by removing the light (L) and heavy (H) chains of the monoclonal antibody as well as water molecules in the structure file. Default Gasteiger charges were assigned to the receptor.

In order to model the Michaelis complex between the α -aminoalkylphosphonate inhibitor and PSA, a slightly modified flexible side chain method for covalent docking was utilized.²⁵ The inhibitors were linked via covalent bond from the OG (oxygen of the hydroxyl group) atom of SER₁₉₅ to the P atom of the inhibitor while removing a phenoxide from the structure to generate the pentavalent phosphorus. Chirality on the phosphorus stereocenter was selected to be the (R)-isomer, in order for the P=O of the phosphonate ester functional group to be in spatial proximity of the amide protons in the oxyanion hole, the likely source for the stabilization of the tetrahedral intermediate. For the docking study, water was chosen as the dummy ligand to calculate the free energy change from the flexible side chain. In order to prevent interactions from the water molecule and the rigid/flexible receptors, a Gaussian map was used to restrain the oxygen atom to the following coordinates: x –65.000, y –37.475, z –21.304. The Gaussian function is employed with zero energy at the designated site using a half-width setting of 5 and an energy barrier height of 1000 kJ. The grid parameters were as follows: box center –36.636, –37.475, –21.304 (x, y, z), box points 126, 100, 100 (x, y, z), and 0.375 Å resolution. The Lamarckian Genetic Algorithm (LGA) search function was used with 2 500 000 energy calculations/run, 25 LGA runs, and with randomized starting position (tran0), orientation (quat0), and dihedrals (dihe0) as well as default Solis–Wets local search options. Flexible side chains with the lowest internal energy were chosen as the covalent binding pose, computationally modeled as the MD-predicted crystal structure of PSA-ligand Michaelis complex. A schematic of ligand binding serving as the basis for modeling the Michaelis complex is shown in Scheme 1.

To model the noncovalent binding of diphenyl α -aminoalkylphosphonates, two methods were employed. The first involved more conventional modeling methods described. First, the covalent map function in AutoDock Tools was utilized as a positional restraint on the phosphorus atom of the ligand in close proximity to the SER₁₉₅:OG atom (coordinates x –36.925, y –35.894, z –20.439) of the protein. The LGA search method was employed by randomizing initial position, orientation, and relative dihedrals. The grid box defining the binding search space was input as x center –36.636, y center –37.475, and z center –21.304 (x, y, z) with 100 points (20 Å) in each dimension and 0.200 Å grid resolution. Default LGA search was used with 25 independent runs with 2 500 000 calculations/run. The second method utilized the covalent ligand (flexible side chain) obtained from the Michaelis complex modeling experiments. The covalent linkage acts as a tether without the use of a Gaussian well. From those structures, the covalently bound ligand was removed from the protein and the diphenyl phenoxide moiety was reestablished, the ligand was minimized using AMBER, and docked into the protein binding site using identical grid parameters. Solis–Wets local minimization was used with 200 000 energy minimiza-

Scheme 1. Proposed Mechanistic Schematic of α -Aminoalkylphosphonate Ester Inhibitor Interaction with Serine Proteases (Reprinted from ref 26. Copyright 1998 American Chemical Society)^a

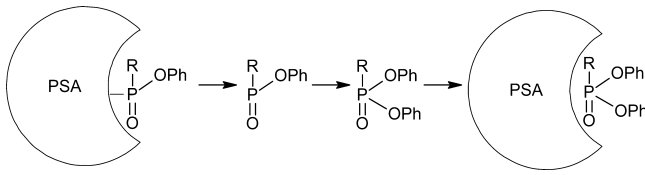


^aThe catalytic triad of ASP₁₀₂, HIS₅₇, and SER₁₉₅ residues of a serine protease are shown above. The non-covalent EI complex (top) reacts with the protease to form the covalent Michaelis complex (middle) in the form of a phenoxymethyleneophosphonate ester, with the transition state stabilized by the oxyanion hole. The monoester (bottom) is the expected product of the acyl-enzyme complex after the loss of the second phenoxide. This scheme was first presented by Jackson and co-workers.²⁶

tions/run and 25 runs, with the upper and lower limit of rho set to 80.0 and 0.01, respectively. Initial position, orientation, and dihedrals were all conserved in these experiments. All other parameters were kept as default. This method is visually summarized in Scheme 2.

2.2. Molecular Dynamics Simulation. MD simulations were performed using GROMACS version 4.6.5²⁷ with the AMBER ff99SB-ILDN force field.²⁸ The S-enantiomer of **11** (referred to here as **S11**) was chosen for the simulations on the

Scheme 2. Visual Representation of Obtaining Noncovalent Binding Structures of Inhibitors from the Michaelis Complex Modeling Results



basis of its AutoDock 4.2 binding score. Ligand parameters were acquired with Antechamber^{29,30} and the AmberTools13 package along with the AM1-BCC method through USCF Chimera to assign partial charges. GROMACS usable topologies were acquired through conversion via ACPYPE.³¹ Ligand topology, including atom type and partial charges, can be found in the Supporting Information (Table S1). Atom parametrization of S11 carbamoyl moiety is within agreement of published results of amides and benzamide.^{32,33}

The PSA protein structure was obtained in the same manner as described in the molecular docking experiments, with the sugar moieties removed for the simulation. The PSA–**S11** complex and PSA were centered in separate cubic boxes and each solvated using the TIP3P³⁴ water model and SPC216³⁵ solvent configuration. Simulation parameters were obtained from AMBER ff99SB-ILDN parametrization procedure and accommodated to fit a standard for both systems. All Histidine residues within the protein structure were kept neutral for the simulation. Histidine residues 25, 48, 70, 75, 87, 91, 101, 161, 172, and 234 were protonated at the N_e atom, and HIS₅₇ was protonated at the N_d position. Charges of anionic/cationic residues assigned to the PSA structure can be found in Table S2. No additional ions were needed for the system to achieve electroneutrality. Short-range nonbonded interaction cutoffs were set to 1.0 nm, while the Particle Mesh Ewald (PME)³⁶ algorithm was executed as the Coulomb-type to calculate long-range electrostatics. Dispersion correction was performed to account for energy and pressure cutoffs due to the Verlet³⁷ cutoff-scheme. Periodic boundary conditions were set to allow free motion along the 3D lattice.

A steepest descent minimization removed improper atom contacts. Convergence was achieved when a maximum force of less than 1000 kJ mol⁻¹ nm⁻¹ resided on any atom. Sequentially, a two-step equilibration phase was used to independently simulate both constant volume (NVT) and constant pressure (NPT) ensembles. NVT ensembles of 50 ps (ps) were simulated for both systems, sustaining the temperature at 310 K, through the utilization of the velocity rescaling³⁸ (v-rescale) thermostat. Protein and solvent atoms were thermally coupled separately. Subsequently, NPT equilibration was isotropically controlled using the Parrinello–Rahman³⁹ barostat. Systems were simulated at intervals of 50 ps until pressures sustained at 1.0 bar with v-rescale thermostat for maintaining 310 K. Following NPT equilibration, MD simulations were conducted for 5 ns using the same conditions as described.

2.3. Synthesis of α -Aminoalkylphosphonate Ester Inhibitors. All chemicals were purchased from Fisher Scientific and were used as received. Deuterated solvents were purchased from Acros Organics. Nuclear magnetic resonance (NMR) spectra for ¹H, ¹³C, and ³¹P nuclei were obtained on Varian INNOVA 300 and 500 MHz NMR spectrometers. Broad-band

proton-decoupled ^{31}P spectra were recorded using 85% phosphoric acid in a sealed capillary as an internal standard. High-resolution mass spectrometry (HRMS) experiments were conducted using Micromass AutoSpec M magnetic sector using chemical ionization (CI) in methane. No effort was made to separate the enantiomers of the products.

Diphenyl [N-Benzylloxycarbonylamino(phenyl)methyl] Phosphonate (Entry 1). A 1:1:1.1 equiv mixture of 110 mg benzaldehyde (1.0 mmol), 150 mg benzyl carbamate (1.0 mmol), and 0.29 mL triphenyl phosphite (1.1 mmol) were partially dissolved in 1 mL glacial acetic acid and heated to reflux for 3 h. After completion, volatiles were removed under reduced pressure to yield a crude product. The crude was dissolved in minimal amount of hot methanol and cooled to 0 °C. The voluminous solid that precipitated out of solution was then collected, filtered, washed with cold methanol, and was subsequently recrystallized in methanol. The product was isolated as a colorless solid (334 mg, 71% yield): ^1H NMR (DMSO, 500 MHz) δ 5.10 (AB_{qt} , $\Delta\nu = 42.0$ Hz, $J = 12.7$ Hz, 2H), 5.60 (dd, $J = 22.1$ Hz and $J = 9.7$ Hz, 1H), 6.95 (d, $J = 8.3$ Hz, 2H), 7.05 (d, $J = 8.8$ Hz, 2H), 7.18–7.20 (m, 2H), 7.31–7.41 (m, 12H), 7.64 (d, $J = 7.3$ Hz, 2H), 8.92 (d, $J = 10.2$ Hz, 1H). ^{13}C NMR (DMSO, 300 MHz) δ 51.84, 53.91, 66.16, 120.22, 120.28, 120.33, 125.21, 125.30, 127.92, 128.24, 128.33, 128.41, 128.55, 129.77, 129.81, 134.33, 136.63, 149.71, 149.85, 150.00, 150.14, 155.93, 156.06. ^{31}P NMR (DMSO, 300 MHz) δ 15.88. HRMS (CI, methane) m/z calculated for $\text{C}_{27}\text{H}_{25}\text{NO}_5\text{P}$ (M + 1) 474.147037, found 474.145015.

Diphenyl [N-Benzylloxycarbonylamino(4-fluorophenyl)methyl] Phosphonate (Entry 2). This compound was prepared in a similar manner as entry 1, from 165 mg 4-fluorobenzaldehyde (1.0 mmol), 150 mg benzyl carbamate (1.0 mmol), and 0.29 mL triphenyl phosphite (1.1 mmol) in 1 mL glacial acetic acid. The product recrystallized at 0 °C from methanol as colorless crystalline needles (350 mg, 66% yield). ^1H NMR (DMSO, 500 MHz) δ 5.11 (AB_{qt} , $\Delta\nu = 41.8$ Hz, $J = 12.7$ Hz, 2H), 5.65 (dd, $J = 22.0$ Hz and $J = 10.2$ Hz, 1H), 6.98 (s, $J = 8.3$ Hz, 2H), 7.06 (d, $J = 8.8$ Hz, 2H), 7.18–7.20 (m, 4H), 7.30–7.38 (m, 9H), 7.70 (ddd, $J = 8.3$ Hz, 5.9 Hz, and 2.0 Hz, 2H), 8.92 (d, $J = 10.2$ Hz, 1H). ^{13}C NMR (DMSO, 300 MHz) δ 51.07, 53.18, 66.19, 115.15, 115.44, 120.19, 120.25, 120.29, 125.24, 125.31, 127.94, 128.33, 129.78, 129.83, 130.55, 130.65, 130.75, 136.59, 149.68, 149.82, 149.97, 150.09, 155.86, 155.98, 160.30. ^{31}P NMR (DMSO, 300 MHz) δ 15.56. HRMS (CI, methane) m/z calculated for $\text{C}_{27}\text{H}_{24}\text{NO}_5\text{PF}$ (M + 1) 492.137615, found 492.139395.

Diphenyl [N-Benzylloxycarbonylamino(4-tert-butylphenyl)methyl] Phosphonate (Entry 3). This compound was prepared in a similar manner as entry 1, from 0.13 mL 4-tert-butylbenzaldehyde (1.0 mmol), 150 mg benzyl carbamate (1.0 mmol), and 0.29 mL triphenyl phosphite (1.1 mmol) in 1 mL glacial acetic acid. The product recrystallized at 0 °C from methanol as fine colorless needles (261 mg, 50% yield): ^1H NMR (DMSO, 500 MHz) δ 1.28 (s, 9 H), 5.09 (AB_{qt} , $\Delta\nu = 40.5$ Hz, $J = 12.4$ Hz, 2H), 5.54 (dd, $J = 22.0$ Hz and $J = 10.2$ Hz, 1H), 6.92 (d, $J = 8.3$ Hz, 2H), 7.04 (d, $J = 8.8$ Hz, 2H), 7.16–7.20 (m, 2H), 7.29–7.38 (m, 9H), 7.40 (d, $J = 8.3$ Hz, 2H), 7.54 (dd, $J = 8.3$ Hz and 2.0 Hz, 2H), 8.86 (d, $J = 10.2$ Hz, 1H). ^{13}C NMR (DMSO, 300 MHz) δ 31.03, 34.29, 51.52, 53.61, 66.12, 120.23, 120.28, 120.34, 125.24, 127.91, 128.21, 128.29, 128.33, 129.75, 131.23, 136.65, 149.89, 150.01, 150.15, 150.72, 150.76, 155.92, 156.03. ^{31}P NMR (DMSO, 300 MHz)

δ 16.03. HRMS (CI, methane) m/z calculated for $\text{C}_{31}\text{H}_{33}\text{NO}_5\text{P}$ (M + 1) 530.209637, found 530.211016.

Diphenyl [N-Benzyloxycarbonylamino(4-hydroxyphenyl)methyl] Phosphonate (Entry 4). This compound was prepared in a similar manner as entry 1, from 610 mg 4-hydroxybenzaldehyde (5.0 mmol), 750 mg benzyl carbamate (5.0 mmol), and 1.45 mL triphenyl phosphite (5.5 mmol) in 2 mL glacial acetic acid. The product recrystallized at 0 °C from ethanol/diethyl ether (3:1) as a colorless solid (1.27 g, 52% yield). ^1H NMR (DMSO, 500 MHz) δ 5.09 (AB_{qt} , $\Delta\nu = 41.0$ Hz, $J = 12.6$ Hz, 2H), 5.46 (dd, $J = 21.6$ Hz and $J = 10.2$ Hz, 1H), 6.77 (d, $J = 8.3$ Hz, 2H), 6.95 (d, $J = 8.3$ Hz, 2H), 7.05 (d, $J = 8.8$ Hz, 2H), 7.19 (td, $J = 7.3$ Hz and 4.4 Hz, 2H), 7.30–7.37 (m, 9H), 7.41 (dd, $J = 8.8$ Hz and 1.9 Hz, 2H), 8.77 (d, $J = 10.2$ Hz, 1H), 9.56 (s, 1H). ^{13}C NMR (DMSO, 300 MHz) δ 51.27, 53.38, 66.09, 115.18, 120.26, 120.33, 120.39, 124.32, 125.13, 125.22, 127.91, 128.33, 129.75, 129.78, 129.91, 136.70, 149.82, 149.94, 150.11, 150.23, 155.89, 156.00, 157.38, 157.41. ^{31}P NMR (DMSO, 300 MHz) δ 16.40. HRMS (CI, methane) m/z calculated for $\text{C}_{27}\text{H}_{25}\text{NO}_6\text{P}$ (M + 1) 490.141951, found 490.141518.

Diphenyl [N-Benzyloxycarbonylamino(4-cyanophenyl)methyl] Phosphonate (Entry 5). This compound was prepared in a similar manner as entry 1, from 1.3 g 4-cyanobenzaldehyde (10.0 mmol), 1.5 g benzyl carbamate (10.0 mmol), and 2.9 mL triphenyl phosphite (11.0 mmol) in 2 mL glacial acetic acid. The product recrystallized at room temperature from dichloromethane/methanol as colorless crystalline needles (3.86 g, 77% yield). ^1H NMR (DMSO, 500 MHz) δ 5.12 (AB_{qt} , $\Delta\nu = 40.4$ Hz, $J = 12.5$ Hz, 2H), 5.81 (dd, $J = 23.3$ Hz and $J = 10.2$ Hz, 1H), 7.02 (d, $J = 8.3$ Hz, 2H), 7.05 (d, $J = 8.3$ Hz, 2H), 7.21 (td, $J = 7.3$ Hz and 3.4 Hz, 2H), 7.32–7.39 (m, 9H), 7.86–7.91 (m, 4H), 9.05 (d, $J = 10.2$ Hz, 1H). ^{13}C NMR (DMSO, 300 MHz) δ 51.68, 53.76, 66.35, 111.09, 118.57, 120.17, 120.23, 120.29, 125.36, 125.47, 127.96, 128.37, 129.34, 129.42, 129.85, 129.92, 132.38, 136.51, 140.05, 149.59, 149.72, 149.86, 150.00, 155.90, 156.01. ^{31}P NMR (DMSO, 300 MHz) δ 14.52. HRMS (CI, methane) m/z calculated for $\text{C}_{28}\text{H}_{24}\text{N}_2\text{O}_5\text{P}$ (M + 1) 499.142286, found 499.143536.

Diphenyl [N-Benzyloxycarbonylamino(4-methoxyphenyl)methyl] Phosphonate (Entry 6). This compound was prepared in a similar manner as entry 1, from 340 mg 4-anisaldehyde (2.5 mmol), 368 mg benzyl carbamate (2.5 mmol), and 0.74 mL triphenyl phosphite (2.8 mmol) in 2 mL glacial acetic acid. The product recrystallized at 0 °C from dichloromethane/methanol as a colorless solid (554 mg, 44%). ^1H NMR (DMSO, 500 MHz) δ 3.76 (s, 3H), 5.10 (AB_{qt} , $\Delta\nu = 40.4$ Hz, $J = 12.7$ Hz, 2H), 5.54 (dd, $J = 22.1$ Hz and $J = 10.2$ Hz, 1H), 6.95–6.98 (m, 4H), 7.06 (d, $J = 8.3$ Hz, 2H), 7.19 (td, $J = 7.3$ Hz and 2.9 Hz, 2H), 7.30–7.38 (m, 9H), 7.56 (dd, $J = 8.3$ Hz and 1.9 Hz, 2H), 8.84 (d, $J = 10.2$ Hz, 1H). ^{13}C NMR (DMSO, 300 MHz) δ 51.20, 53.29, 55.13, 66.10, 113.84, 120.23, 120.29, 120.36, 125.15, 125.24, 126.12, 127.91, 128.33, 129.75, 129.80, 129.86, 136.67, 149.77, 149.91, 150.06, 150.20, 155.89, 156.00, 159.15. ^{31}P NMR (DMSO, 300 MHz) δ 16.15. HRMS (CI, methane) m/z calculated for $\text{C}_{28}\text{H}_{26}\text{NO}_6\text{P}$ (M+) 503.149776, found 503.149148.

Diphenyl [N-Benzyloxycarbonylamino(4-(dimethylamino)phenyl)methyl] Phosphonate (Entry 7). This compound was prepared in a similar manner as entry 1, from 750 mg 4-(dimethylamino)benzaldehyde (5.0 mmol), 750 mg benzyl carbamate (5.0 mmol), and 1.45 mL triphenyl phosphite (5.5 mmol) in 1.5 mL glacial acetic acid. The

product recrystallized at 0 °C from methanol as colorless needles (812 mg, 31% yield): ^1H NMR (DMSO, 500 MHz) δ 2.89 (s, 6H), 5.09 (AB_{qt} , $\Delta\nu = 38.5$ Hz, $J = 12.7$ Hz, 2H), 5.42 (dd, $J = 21.1$ Hz and $J = 10.2$ Hz, 1H), 6.71 (d, $J = 8.8$ Hz, 2H), 6.96 (d, $J = 7.8$ Hz, 2H), 7.06 (d, $J = 8.3$ Hz, 2H), 7.18 (td, $J = 7.3$ Hz and 3.4 Hz, 2H), 7.31–7.37 (m, 9H), 7.41 (dd, $J = 8.8$ Hz and 1.9 Hz, 2H), 8.74 (d, $J = 10.2$ Hz, 1H). ^{13}C NMR (DMSO, 300 MHz) δ 51.26, 53.36, 66.03, 112.03, 120.26, 120.36, 120.42, 121.04, 125.07, 125.18, 127.88, 128.32, 129.24, 129.33, 129.72, 129.77, 136.73, 149.85, 149.98, 150.14, 150.26, 155.87, 156.00. ^{31}P NMR (DMSO, 300 MHz) δ 16.41. HRMS (CI, methane) m/z calculated for $\text{C}_{28}\text{H}_{25}\text{NO}_7\text{P}$ (M+) 516.181411, found 516.182187.

Diphenyl [N-Benzylloxycarbonylamino(4-(methylsulfonyl)-phenyl)methyl] Phosphonate (Entry 8). This compound was prepared in a similar manner as entry 1, from 185 mg 4-(methylsulfonyl)benzaldehyde (1.0 mmol), 150 mg benzyl carbamate (1.0 mmol), and 0.29 mL triphenyl phosphite (1.1 mmol) in 2 mL glacial acetic acid. The product recrystallized at 0 °C from methanol as fine colorless needles (355 mg, 65% yield): ^1H NMR (DMSO, 500 MHz) δ 3.23 (s, 3 H), 5.11 (AB_{qt} , $\Delta\nu = 38.9$ Hz, $J = 12.3$ Hz, 2H), 5.80 (dd, $J = 22.6$ Hz and $J = 10.2$ Hz, 1H), 7.02 (d, $J = 7.8$ Hz, 2H), 7.07 (d, $J = 8.8$ Hz, 2H), 7.20 (t, $J = 7.7$ Hz, 2H), 7.32–7.38 (m, 9H), 7.92 (dd, $J = 8.2$ Hz and 1.6 Hz, 2H), 7.96 (d, $J = 8.3$ Hz, 2H), 9.06 (d, $J = 9.7$ Hz, 1H). ^{13}C NMR (DMSO, 300 MHz) δ 43.37, 51.58, 53.65, 66.32, 120.17, 120.23, 120.31, 125.34, 125.45, 127.05, 127.95, 128.35, 129.30, 129.36, 129.83, 129.91, 136.51, 140.30, 140.57, 140.62, 149.59, 149.71, 149.86, 150.00, 155.90, 156.01. ^{31}P NMR (DMSO, 300 MHz) δ 15.31. HRMS (CI, methane) m/z calculated for $\text{C}_{28}\text{H}_{27}\text{NO}_7\text{PS}$ (M + 1) 552.124588, found 552.122968.

Diphenyl [N-Benzylloxycarbonylamino(4-methoxy-carbonylphenyl)methyl] Phosphonate (Entry 9). This compound was prepared in a similar manner as entry 1, from 165 mg methyl-4-formylbenzoate (1.0 mmol), 150 mg benzyl carbamate (1.0 mmol), and 0.29 mL triphenyl phosphite (1.1 mmol) in 1 mL glacial acetic acid. The product recrystallized at 0 °C from dichloromethane/methanol as colorless crystalline needles (350 mg, 66% yield): ^1H NMR (DMSO, 500 MHz) δ 3.86 (s, 3H), 5.11 (AB_{qt} , $\Delta\nu = 41.5$ Hz, $J = 12.5$ Hz, 2H), 5.74 (dd, $J = 23.1$ Hz and $J = 10.2$ Hz, 1H), 7.01 (d, $J = 8.3$ Hz, 2H), 7.06 (d, $J = 8.8$ Hz, 2H), 7.18–7.21 (m, 2H), 7.32–7.38 (m, 9H), 7.80 (dd, $J = 8.8$ Hz and 1.9 Hz, 2H), 7.99 (d, $J = 8.3$ Hz, 2H), 9.03 (d, $J = 10.2$ Hz, 1H). ^{13}C NMR (DMSO, 300 MHz) δ 51.72, 52.19, 53.78, 66.26, 120.19, 120.23, 120.31, 125.28, 125.39, 127.92, 128.33, 128.73, 128.81, 129.19, 129.39, 129.42, 129.80, 129.88, 136.54, 139.73, 149.60, 149.74, 149.89, 150.03, 155.93, 156.04, 165.84. ^{31}P NMR (DMSO, 300 MHz) δ 14.92. HRMS (CI, methane) m/z calculated for $\text{C}_{29}\text{H}_{27}\text{NO}_7\text{P}$ (M + 1) 532.152516, found 532.151548.

Diphenyl [N-Benzylloxycarbonylamino(4-carboxyphenyl)-methyl] Phosphonate (Entry 10). This compound was prepared in a similar manner as entry 1, from 750 mg 4-carboxybenzaldehyde (5.0 mmol), 750 mg benzyl carbamate (5.0 mmol), and 1.45 mL triphenyl phosphite (5.5 mmol) in 10 mL glacial acetic acid. The product recrystallized at 0 °C from methanol as a colorless solid (1.47 g, 57% yield); ^1H NMR (DMSO, 500 MHz) δ 5.11 (AB_{qt} , $\Delta\nu = 40.7$ Hz, $J = 12.6$ Hz, 2H), 5.72 (dd, $J = 23.1$ Hz and $J = 10.2$ Hz, 1H), 7.00 (d, $J = 8.3$ Hz, 2H), 7.06 (d, $J = 8.3$ Hz, 2H), 7.18 (m, 2H), 7.30–7.38 (m, 9H), 7.77 (dd, $J = 8.5$ Hz and 1.7 Hz, 2H), 7.96 (d, $J = 8.3$ Hz, 2H), 9.02 (d, $J = 10.2$ Hz, 1H), 13.03 (s, 1H). ^{13}C NMR

(DMSO, 300 MHz) δ 51.73, 53.82, 66.27, 120.20, 120.26, 120.33, 125.31, 125.41, 127.94, 128.37, 128.58, 128.66, 129.36, 129.83, 129.89, 130.65, 136.57, 139.23, 149.63, 149.77, 149.92, 150.06, 155.95, 156.06, 166.93. ^{31}P NMR (DMSO, 300 MHz) δ 14.95. HRMS (CI, methane) m/z calculated for $\text{C}_{28}\text{H}_{25}\text{NO}_7\text{P}$ (M + 1) 518.136866, found 518.137054.

Diphenyl [N-Benzylloxycarbonylamino(4-carbamoyl-phenyl)methyl] Phosphonate (Entry 11). Compound 2 (360 mg, 0.70 mmol) and di-*tert*-butyldicarbonate (450 mg, 2.06 mmol) were partially dissolved in 12 mL THF/1 mL pyridine and stirred at 50 °C for 30 min, after which the starting material completely dissolved into the reaction mixture. Ammonium carbonate (400 mg, 4.16 mmol) was added to the reaction vessel and the solution was stirred for an additional 6 h under identical conditions. After completion, solvents were removed under rotatory evaporation and the solid residue was suspended in methanol. The solution was stirred upon gentle heating until dissolution to remove excess ammonia and the solvent volume was reduced. The product precipitated out of solution at -16 °C and was subsequently recrystallized from methanol at 0 °C as fine white crystals (270 mg, 75%): ^1H NMR (DMSO, 500 MHz) δ 5.11 (AB_{qt} , $\Delta\nu = 40.1$ Hz, $J = 12.4$ Hz, 2H), 5.68 (dd, $J = 22.9$ Hz and $J = 10.2$ Hz, 1H), 6.99 (d, $J = 7.8$ Hz, 2H), 7.05 (d, $J = 8.8$ Hz, 2H), 7.20 (t, $J = 7.4$ Hz, 2H), 7.31–7.38 (m, 9H), 7.40/7.99 (s, cis/trans, 2H), 7.72 (dd, $J = 8.7$ Hz and 1.9 Hz, 2H), 7.88 (d, $J = 8.3$ Hz, 2H), 8.96 (d, $J = 10.2$ Hz, 1H). ^{13}C NMR (DMSO, 300 MHz) δ 51.65, 53.74, 66.24, 120.20, 120.26, 120.34, 125.28, 125.39, 127.54, 127.94, 128.26, 128.37, 129.81, 129.89, 134.12, 136.59, 137.46, 149.65, 149.79, 149.95, 150.08, 155.93, 156.04, 167.44. ^{31}P NMR (DMSO, 300 MHz) δ 14.99. HRMS (CI, methane) m/z calculated for $\text{C}_{28}\text{H}_{26}\text{N}_2\text{O}_6\text{P}$ (M + 1) 517.152850, found 517.152278.

Diphenyl [N-Benzylloxycarbonylamino(4-nitrophenyl)-methyl] Phosphonate (Entry 12). This compound was prepared in a similar manner as entry 1, from 1.5 g of 4-nitrobenzaldehyde (10.0 mmol), 1.5 g benzyl carbamate (10.0 mmol), and 2.9 mL triphenyl phosphite (11.0 mmol) in 4 mL glacial acetic acid. The product recrystallized from dichloromethane/methanol at 0 °C as a colorless solid (3.66 g, 71% yield): ^1H NMR (DMSO, 500 MHz) δ 5.11 (AB_{qt} , $\Delta\nu = 39.2$ Hz, $J = 12.7$ Hz, 2H), 5.87 (dd, $J = 23.3$ Hz and $J = 10.6$ Hz, 1H), 7.03 (d, $J = 8.3$ Hz, 2H), 7.06 (d, $J = 8.3$ Hz, 2H), 7.21 (m, 2H), 7.32–7.38 (m, 9H), 7.95 (dd, $J = 8.8$ Hz and 1.9 Hz, 2H), 8.28 (d, $J = 8.8$ Hz, 2H), 9.10 (d, $J = 10.2$ Hz, 1H). ^{13}C NMR (DMSO, 300 MHz) δ 51.52, 53.59, 66.35, 120.17, 120.23, 120.26, 120.33, 123.50, 123.53, 125.38, 125.47, 127.95, 128.35, 129.65, 129.72, 129.85, 129.92, 136.50, 142.08, 147.30, 147.34, 149.56, 149.69, 149.83, 149.97, 155.90, 156.03. ^{31}P NMR (DMSO, 300 MHz) δ 14.40. HRMS (CI, methane) m/z calculated for $\text{C}_{27}\text{H}_{24}\text{N}_2\text{O}_7\text{P}$ (M + 1) 519.132115, found 519.131005.

Diphenyl [N-Benzylloxycarbonylamino(4-aminophenyl)-methyl] Phosphonate (Entry 13). A 1.03 g (2 mmol) portion of 12 was added to a round-bottom flask containing 6 mL ethanol and 6 mL glacial acetic acid and was placed under gentle heating until dissolution. A 2 g portion of zinc dust was added to the solution and heated to reflux overnight. The resulting mixture was filtered and the filtrate solvent was removed under reduced pressure. The residue was dissolved in ethyl acetate and washed with saturated sodium bicarbonate solution ($\times 3$). The organic layer was extracted, dried with magnesium sulfate, filtered, and the solvent was reduced under vacuum. The sample was triturated with diethyl ether to afford

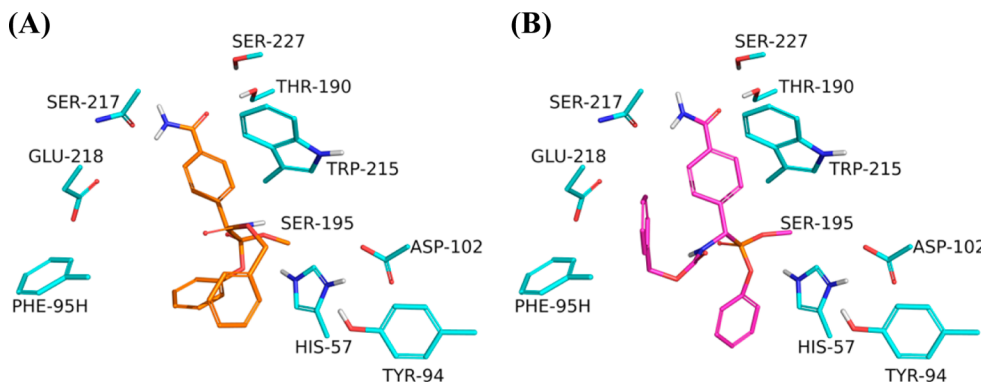


Figure 2. Covalent binding model of diphenyl [N-benzyloxycarbonylamino(4-carbamoylphenyl)methyl] phosphonate in PSA using the flexible side chain method in AutoDock4. (A) S-Enantiomer of the inhibitor with the N-blocking group in the P2 pocket of the protein, in proximity to TYR₉₄. (B) R-Enantiomer model showing nearly the same orientation except with the N-blocking group in the upper groove region near TRP₂₁₅. AutoDock models are consistent with previous X-ray data of diphenyl phosphonate ester derivatives and serine proteases by Bertrand et al.¹⁸

a solid, which was subsequently filtered and recrystallized with methanol/diethyl ether at -16 °C to yield the product as a yellow solid (805 mg, 83%): ¹H NMR (DMSO, 500 MHz) δ 3.60 (s, br), 5.11 (AB_{qt}, Δν = 41.8 Hz, J = 11.7 Hz, 2H), 5.65 (dd, J = 22.1 Hz and J = 10.2 Hz, 1H), 6.99 (d, J = 8.3 Hz, 2H), 7.06 (d, J = 8.3 Hz, 2H), 7.20 (t, J = 7.3 Hz, 2H), 7.31–7.41 (m, 11H), 7.72 (dd, J = 8.3, 1.9 Hz, 2H), 8.95 (d, J = 10.2 Hz, 1H). ¹³C NMR (DMSO, 300 MHz) δ 51.36, 53.45, 66.26, 120.22, 120.29, 120.36, 122.60, 125.30, 125.41, 127.95, 128.37, 129.71, 129.83, 129.91, 133.31, 136.59, 149.65, 149.79, 149.94, 150.08, 155.92, 156.04. ³¹P NMR (DMSO, 300 MHz) δ 15.18. HRMS (CI, methane) *m/z* calculated for C₂₇H₂₅N₂O₅P (M+) 488.150111, found 488.151111.

2.4. Inhibition Kinetics Assays. Human PSA protein was purchased from Fitzgerald (Catalog no. 30-AP14). Chromogenic substrate MeO-Suc-Arg-Pro-Tyr-pNA-HCl (S-2586) was purchased from DiaPharma. Absorbance readings were conducted using Tecan Infinite M200 well plate reader. Sterile polystyrene-based flat bottom 96 well plates were obtained from Corning.

In typical experiments, a 10 μL aliquot of varying concentrations of inhibitor solutions (prepared in 99.7% dimethyl sulfoxide, DMSO) were added to 75 μL protein buffer solution (5 μg PSA protein in 100 mM Tris-HCl, 1.5 M NaCl, pH 7.5) in a 96-well plate. After a 20 min preincubation at 37 °C, 15 μL of the substrate S-2586 in Tris buffer was added for a total concentration of 1 mM and a total volume of 100 μL in each well. Amidolytic activity of PSA was measured by cleavage of the substrate to yield *p*-nitroaniline analyte, recording absorbance at 405 nm for 60 min. To determine inhibitor potency, enzymatic activities of inhibited and noninhibited PSA kinetic readings were compared and the estimated IC₅₀ values were calculated using the four-point log (4PL) transformation analysis of the inhibitor concentration vs enzymatic activity.

3. RESULTS AND DISCUSSION

3.1. AutoDock Ligand Binding Structure Determination. Although mechanisms of binding of diphenyl aminoalkylphosphonates with select proteases have been reported, the extent of the research is limited and none have been demonstrated with the PSA enzyme. Bertrand et al. published X-ray structure and computational models for the compound diphenyl [N-benzyloxycarbonylamino(4-amidinophenyl)-

methyl] phosphonate and its intermediates. The authors describe the crystal structure of the inhibitor covalently bound to bovine pancreatic trypsin and used the molecular modeling via CHAIN docking algorithm. The ligand was incrementally docked into human thrombin protein via superposition in order to deconvolute inhibitor intermediates and their binding modes.¹⁸ The work published provided fundamental insight in the determination of the covalent Michaelis complex of the bound inhibitor as well as localization of inhibitor moieties within the binding site of the serine proteases. In addition, the work from Bertrand and colleagues was used as a homology model to optimize covalent binding of this class of compounds using AutoDock.

To accumulate binding structures of diphenyl aminoalkylphosphonates derivatives, we employed a unique method to determine docking conformations. Due to the rather large solvent-accessible volume surrounding the catalytic triad of PSA, nonconstrained standard docking procedures would yield a myriad of binding conformations when using LGA search, despite the number of LGA runs or energy calculations. As a consequence, major clusters of binding poses within 2.0 Å could not be obtained and resulted in at least several clusters that deviated greatly from one another. This is not only due to the aforementioned binding space of PSA, but also the number of rotatable torsions allowed for the ligand, which further complicates the computationally exhaustive search.

In order to model the Michaelis complex of the bound inhibitor, the flexible side chain parameters of AutoDock was exploited as a covalent tether constraint. The flexible side chain method has a couple distinct advantages; it avoids the clash penalty that arises from neighboring atoms when using a single Gaussian map and keeps the scoring function intact while modeling a bound conformation of the inhibitor to the protein. Inhibitory compounds were constructed into the binding site of PSA via covalent linkage between SER₁₉₅ and the phosphonate moiety of the inhibitor (Figure 2). Using a position-constrained water molecule as a dummy ligand, Michaelis complexes of PSA were minimized and the ligands were determined using LGA search and AutoDock 4.2 scoring function. Poses generated were not only consistent with the general placement of moieties seen in homologue models,¹⁸ top hits from individual runs had clustered better than using a Gaussian constraint alone on the ligand to SER₁₉₅. Noncovalent ligand poses were generated by first cleaving the ligand side chain from the SER₁₉₅ residue, and then constructing the diphenylphosphonate ester moiety.

Noncovalent ligand searches were performed using a local search and the AutoDock scores are summarized in Table 1. All

Table 1. AutoDock Noncovalent Binding Scores of 13 Diphenylphosphonate Ester Compounds Selected and Their Stereoisomers and IC₅₀ Concentrations As a Comparison^a

compound	R-group	binding score (kJ/mol)	IC ₅₀
1	H	R: -6.82	79.9 μM
		S: -7.41	
2	F	R: -7.07	43.4% @250 μM
		S: -7.43	
3	C(CH ₃) ₃	R: -4.70	53.2% @250 μM
		S: -6.06	
4	OH	R: -8.12	7.0 μM
		S: -8.42	
5	CN	R: -8.14	68.8% @250 μM
		S: -7.97	
6	OCH ₃	R: -7.55	40.8 μM
		S: -6.61	
7	N(CH ₃) ₂	R: -6.86	77.4 μM
		S: -6.67	
8	SO ₂ CH ₃	R: -7.11	77 μM
		S: -6.45	
9	CO ₂ CH ₃	R: -7.03	91.9 μM
		S: -7.32	
10	CO ₂ H	R: -7.63	7.8 μM
		S: -7.89	
11	CONH ₂	R: -8.29	0.25 μM
		S: -9.14	
12	NO ₂	R: -6.92	137 μM
		S: -6.63	
13	NH ₂	R: -7.51	16.7 μM
		S: -7.65	

^aIC₅₀ values were obtained from the racemic mixture of each compound.

ligand docking experiments were performed with the major ionization state of each ligand at biological pH. It must be noted that the result of the flexible side chain/dummy ligand experiment does not provide free energy scores. Covalent binding structures were sorted by intramolecular energies calculated between the covalently linked ligand and the protein. Top Michaelis complex structures were selected, the ligand was cleaved from the protein, rebuilt, minimized locally, and redocked as a noncovalent molecule to obtain comparable docking scores.

Due to the chiral center involved, compounds isolated from reaction steps are racemic mixtures. As a consequence, both R- and S-enantiomers of the designed compounds were scored using AutoDock. Although the enantiomers have scores that differ from one another, more notably the S-enantiomers score generally higher, the overall trend in ranking of molecules and their respective scores remains the same (i.e., **11** scoring highest for both stereoisomers, **3** the lowest). The difference can be attributed to the summation of favorable and nonfavorable interactions between non-S1 moieties, which were observed by slight variations in arrangement in space. Both enantiomer scores were within 1 kJ/mol from one another, with the exception being **3**.

The compounds selected were chosen based on their variety of functional groups in order to investigate their interactions with the P1 pocket residues. It was determined by the docking studies that **11** had scored the highest out of the compounds chosen for this study, with a free energy score of -8.29/-9.14 kJ·mol⁻¹ for R/S, respectively. Both stereoisomers were consistent with respect to their interactions between the P1 pocket residues of THR₁₉₀, SER₂₁₇, and SER₂₂₇ and the carbamoyl moiety of the ligand (Figure 3). The model predicts that both hydroxyls of THR₁₉₀ and SER₂₂₇ form hydrogen bonds with the C=O of the carbamoyl, with distances of 2.2 and 2.5 Å, respectively. Concurrently, the amide proton forms a 2.2 Å hydrogen bond with the carbonyl of the SER₂₁₇ amide. This push–pull hydrogen bonding between the S1/P1 groups

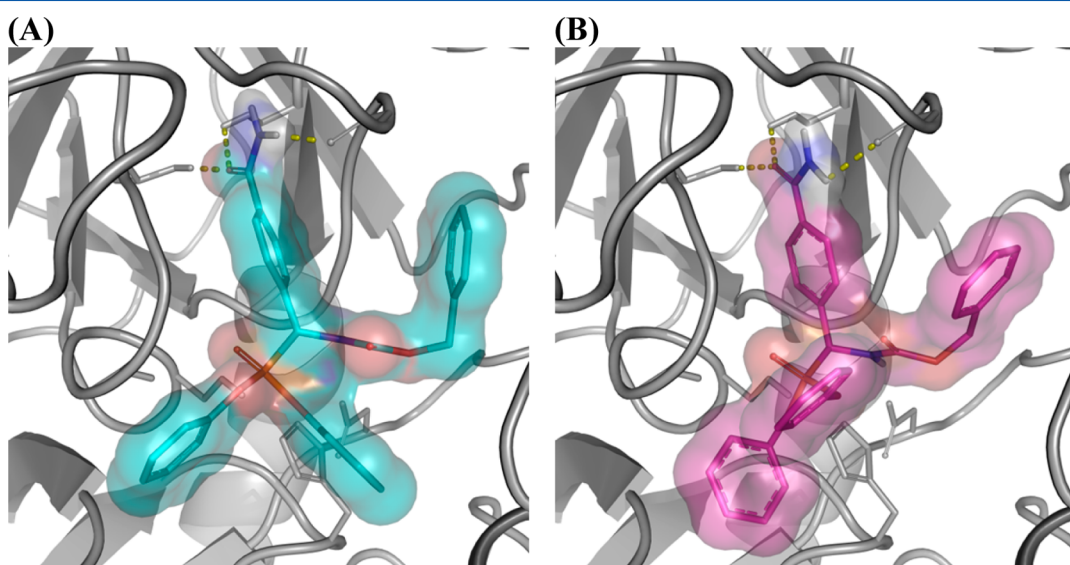


Figure 3. Noncovalent docking of diphenyl [N-benzyloxycarbonylamino(4-carbamoylphenyl)methyl] phosphonate and polar hydrogen contacts (yellow) of selected residues (red) within P1 pocket of PSA. Amide proton of THR₁₉₀ and hydroxyl proton of SER₂₂₇ display hydrogen-bonding contacts with the C=O of the amide functional group of the inhibitor, while the carbonyl of SER₂₁₇ displays a hydrogen-bonding contact with the amide protons of the inhibitor for both the (A) R- and (B) S-enantiomer.

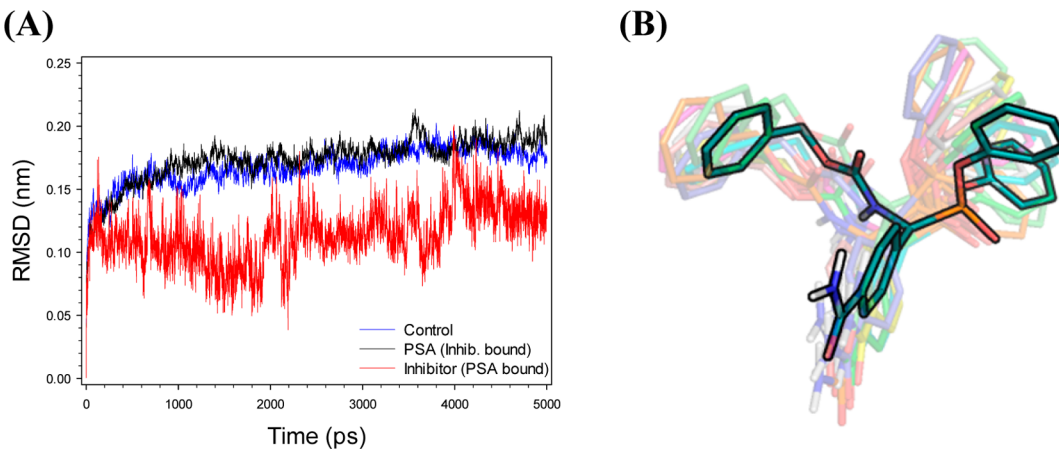


Figure 4. (a) RMSD plots of PSA-S11 complex and PSA alone. (b) Trajectory overlay of S11 over the 5 ns simulation.

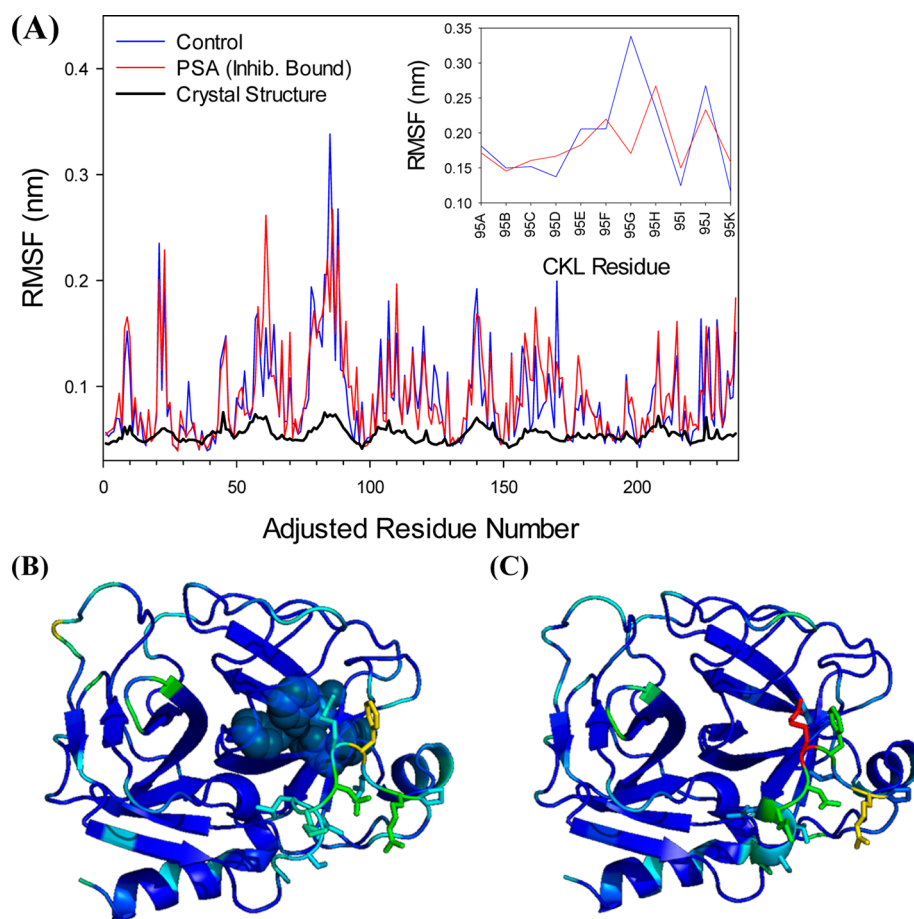


Figure 5. (a) Root-mean squared fluctuations (RMSF) of the 237 residues of PSA with the CKL residues shown in the inset. RMSF representations of the protein (a) with and (b) without S11 bound. Color scale: >0.30 nm red; >0.25 nm yellow; >0.20 nm green; >0.15 nm cyan; <0.15 nm blue. CKL side chains are displayed only. The ligand is represented as blue spheres.

of the inhibitor/protein is what is thought to stabilize the binding conformation.

As a comparison, a tyrosine-like analogue **4** was constructed to compare ligand binding poses. The compound was modeled to show similar hydrogen-bonding interactions with P1 residues, although not to the same extent as **11**. The compound still obtained a significant score of $-8.12/-8.42 \text{ kJ}\cdot\text{mol}^{-1}$ for the R/S enantiomers, respectively. Compound **10** scored third, with R/S scores of $-7.63/-7.89 \text{ kJ}\cdot\text{mol}^{-1}$. All three compounds

displayed favorable polar interactions with P1 residues. Ligands with bulkier groups at the para-position of the phenyl ring scored worse, due to steric clashing within the binding space of the P1 pocket. As a consequence, ligands **3**, **7**, and **8** scored lower due to the van der Waals term penalty.

Compound **5**, which contains a cyano moiety, was predicted to have a strong affinity to the P1 site. According to the computational work, it predicts the likelihood of a polar interaction between SER₁₈₉ and THR₁₉₀ hydroxyls and the

nitrile group. It is the highly polar nature of the cyano group within the environment of the polar P1 pocket that resulted in significant scores of $-7.97/-8.14\text{ kJ}\cdot\text{mol}^{-1}$ (R/S). It was believed that the compound could potentially show significant inhibition of PSA, however, this was not the case experimentally. The explanation can be found in the end of this article. Overall, the flexible side chain method provided results that resembled crystallographic structures in homology models previously published (Figure S1).¹⁸

3.2. MD Trajectories. MD simulations presented here were performed using the GROMACS bundle. The starting ligand binding pose of **11** was taken from AutoDock molecular docking screens, choosing the more optimal S-enantiomer (will be referred to as **S11** for this section). Compound **S11** was modeled dynamically to test its overall binding stability, deviations of protein structure, fluctuations of local residues, and the retention of ligand hydrogen bond contacts.

To validate the stability of the binding complex, MD analyses were performed using the Visual Molecular Dynamics (VMD) package⁴⁰ and the trajectory tools provided by GROMACS. Root-mean squared deviation of the PSA–**S11** complex and PSA control are shown in Figure 4. In both simulations, global protein trajectories are nearly identical in the retention of the folded PSA structure. The average root-mean squared deviation (RMSD) trajectory values are below 0.20 nm for PSA with the inhibitor retained in the binding cavity. **S11** retains localization of its moieties within the binding cavity of PSA. The *p*-carbamoylphenyl group is highly retained in the P1 pocket with very little fluctuation and no significant torsion twists. The N-carboxybenzyl (Cbz) side group is conserved through the Classic Kallikrein Loop (CKL) toward the P3 site of PSA. The diphenoxyl groups of **S11** deviate significantly throughout the simulation due to high solvent accessibility and very little interaction with PSA to stabilize its local trajectory.

Secondary structure changes were closely observed during the simulation, but no substantial early folding events were found. However, during the simulations of PSA and PSA–**S11**, the secondary structure of the CKL region temporary shifts between 3 and 10 helices to alpha helices/loops. Previous reports have shown that solvent accessibility, starting conformation of the protein (open or closed loop), interactions with neighboring residues, and substrate binding could be responsible for the observed CKL trajectories.⁴¹

Root-mean squared fluctuation (RMSF) plots were taken to compare side chain trajectory changes upon ligand binding. Overall, RMSF of both simulations are very similar, as shown in Figure 5. The exception to this is ARG_{95G}, a CKL residue, and it is involvement in the PSA–**S11** complex was notable when comparing the two simulations. The RMSF of the CKL was significant in both runs, but ARG_{95G} fluctuated significantly less with **S11** bound. The RMSF of the residue was 0.34 and 0.17 nm for the unbound and bound runs, respectively. ARG_{95G}, a highly polar amino acid, would be expected to fluctuate tremendously with high solvent accessibility but this movement is reduced in the presence of **S11**. This can be attributed to a hydrogen bonding contact between the proton-donating guanidine and the carbonyl of the Cbz protecting group (noted here as ^{Cbz}CONH). The prevalence of these hydrogen bonding contacts are shown in Table 2. During the course of the simulation, the carbonyl group hydrogen bonds with the terminal and internal amines of the residue with a prevalence of 62.8% and 12.4%, respectively. Taking these contacts into consideration, reduction of the RMSF of ARG_{95G} upon ligand

Table 2. Hydrogen-Bond Prevalence Map between **S11 and PSA during the 5 ns MD Simulation^a**

H-donor	donor atom	H-acceptor	acceptor atom	% existence
ligand	^{Cbz} CONH	SER ₂₁₄	CONH	47.071
ligand	^{Aryl} CONH ₂	THR ₁₉₀	CONH	7.259
ligand	^{Aryl} CONH ₂	SER ₁₉₂	OH	5.679
ligand	^{Aryl} CONH ₂	SER ₂₁₇	CONH	28.454
ARG _{95G}	NHC(NH ₂) ₂ ⁺	ligand	^{Cbz} CONH	12.418
ARG _{95G}	NHC(NH ₂) ₂ ⁺	ligand	^{Cbz} CONH	62.827
THR ₁₉₀	OH	ligand	^{Aryl} CONH ₂	20.396
GLY ₁₉₃	CONH	ligand	PO(OPh)	59.588
GLY ₁₉₃	CONH	ligand	PO(OPh)	4.179
SER ₁₉₅	OH	ligand	PO(OPh)	2.699
SER ₂₂₇	OH	ligand	^{Aryl} CONH ₂	61.588

^aInteracting atom pairs are in bold.

binding may play a role in binding stability. B-Factors from the crystal structure of PSA were compared to our MD studies display good qualitative agreement in RMSF of residues.

Additionally, the frequency of S1/P1 hydrogen bonding interactions were mapped during the simulations. The purpose was to observe the retention of these contacts that were initially observed during the docking simulations, which provide only a static map of the interactions. Specifically, hydrogen bonding between P1 residues THR₁₉₀, SER₂₁₇, and SER₂₂₇ and the carbamoyl moiety (noted here as ^{Aryl}CONH₂) of the ligand were thought to be exclusively involved. The PSA–**S11** hydrogen bond map was relatively consistent with the polar contacts observed in AutoDock with all three aforementioned residues in the P1 site. Some interactions were mostly conserved during the simulation time, such as the 61.6% prevalence between the hydroxyl group of SER₂₂₇ and the carbonyl (^{Aryl}CONH₂) of **S11**. Some interactions were moderately retained during the simulation time, such as residue interactions with THR₁₉₀ and SER₂₁₇, with hydrogen bonding contact incidences of 20.4% and 28.4%, respectively. Contacts with low frequency of occurrence within the P1 pocket include some contacts not mapped during the docking simulations, such as SER₁₉₂. We believe that this incidental contact is not a major contributor to the stabilization of the binding complex, due to its location on the outer P1 pocket. Additionally, hydrogen bonding between GLY₁₉₃ and the phosphonate ester were highly conserved during the simulation, contributing to the retained trajectory of moiety to its local environment despite high solvent accessibility.

The MD trajectories are within expectations, as previously published in analogous kallikrein models.¹⁸ Interactions with P1 residues are retained during the course of the simulation with no significant ligand conformational changes evidenced. The stability of this complex throughout the duration of the simulation gives credence to the proposed binding orientation in the pose space, as well as insight into the dynamics of the local chemical environment upon ligand binding.

3.3. Synthesis of Compounds. The synthesis of diphenyl α -aminoalkylphosphonates followed a facile Kabachnik-Fields reaction using a 3-component, 2-step, one-pot synthesis consisting of a para-substituted benzaldehyde, benzyl carbamate, and triphenylphosphite. With low solvent volume within the reaction mixture, the crude product precipitates out of solution after a given amount of time. Compounds **5**, **7**, and **12** were initially obtained as oily residues, which were dissolved in

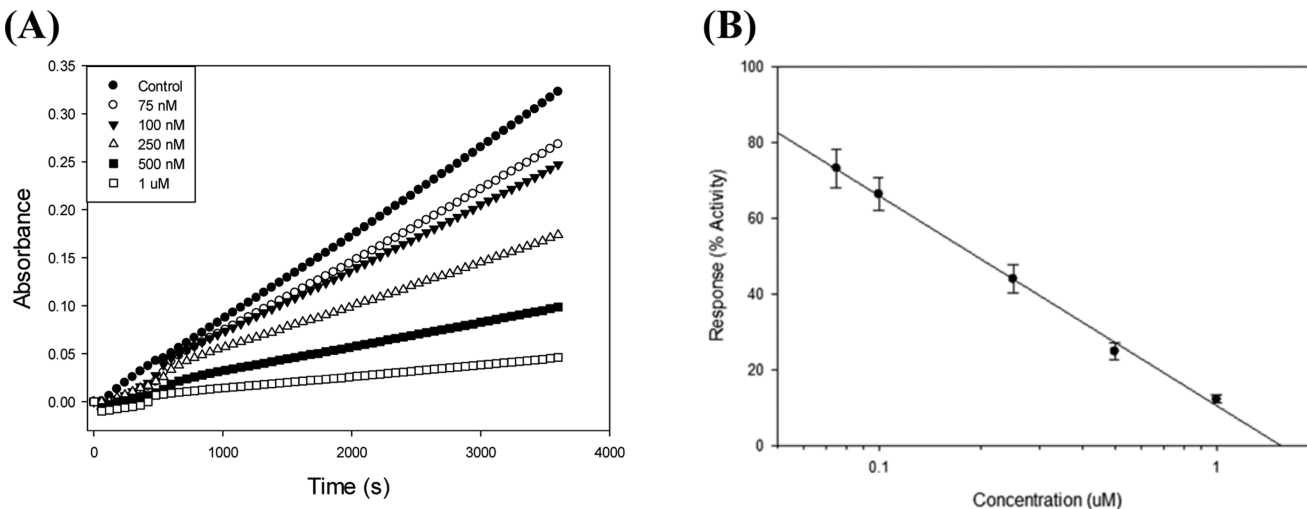


Figure 6. Kinetic assay results of PSA amidolytic activity of chromogenic substrate S-2586 in the presence of varying concentrations of inhibitor 11 from 75 nM to 1 μ M.

the appropriate solvent and cooled to promote crystallization or precipitation. Yields obtained in the reaction were similar to that previously published in literature.^{42–44}

As mentioned, no attempt was made to separate the stereoisomers from the racemic mixture. Compounds were used in the kinetic assays once deemed spectroscopically pure using NMR and mass spectrometry. Completion of the reaction can be monitored by ^1H NMR by observing doublet–doublet signal at 5.0–6.0 ppm range. The signal contains $J_{\text{P}-\text{H}}$ of \sim 22 Hz for heteronuclear coupling and $J_{\text{CH}-\text{NH}} = 10.2$ Hz for proton-to-proton coupling, as expected in previous studies on the reaction-type.⁴⁵ ^1H AB_qt splitting patterns arising from diastereotopic methylene hydrogens were also evident in the NMR spectra as indicative of reaction completion. Heteronuclear coupling of the phosphorus to carbon atoms was also observed in the ^{13}C NMR. Long-range ^{13}C – ^{31}P couplings were observed and reported here, although no attempt was made to assign the signals to carbon atoms in the molecule. ^{13}C signal splitting by ^{31}P nuclei in the carbon NMR can be seen up through four bonds or more,⁴⁶ which makes assignment difficult in this case.

3.4. Dose-Dependent Response Assays. To assess inhibitor potency on PSA, kinetic assays were conducted using chromogenic substrate S-2586 as a method to measure peptide cleavage via p-nitroaniline as a product formation, the liberated chromophore. Dose-dependent response curves were obtained by measuring enzymatic activity of PSA with a dose of substrate and inhibitor. The control in these experiments were represented by the average kinetic rate of substrate cleavage with a blank dose of DMSO. IC₅₀ values were calculated based on the average enzymatic rate of PSA as compared to the control. Final values were estimated using the 4-point log (4PL) method to determine concentrations at which 50% PSA activity inhibition can be extrapolated from the response curves.

The kinetic response curves for PSA with varying doses of the synthesized inhibitors (R/S mixture) were measured. As one example, Figure 6 shows the kinetic response curve for **11**. By varying inhibitor concentrations from 75 nM to 1 μ M, a clear dose-dependent response can be obtained. Concentrations chosen to calculate IC₅₀ values were determined by initially measuring PSA activities using total inhibitor concentrations ranging from 75 nM to 250 μ M. Subsequent

assays were performed to optimally determine concentrations closest to the inflection point in order to properly estimate IC₅₀ values using the 4PL method. Plateau values of the sigmoidal curve where dose concentrations correlated with approximately zero or 100% activity observed were avoided in order to properly use the logistic function. Methods described here have been used in other similar systems.⁴⁷

From using the 4PL method to determine IC₅₀ values, a broad range of potencies was observed from this selective class of compounds (Table 1). Initially, it was believed that compound **4** would show the most potent dose-dependent inhibition of PSA based on previous work performed on tyrosine-containing analogs and peptides or inhibitors containing a *p*-hydroxyphenyl moiety and its specificity to the P1 site. According to its concentration response curve, compound **4** demonstrated only modest inhibition of PSA with an IC₅₀ of 7.0 μ M. From the set of inhibitors, **4** tested as the second-most potent inhibitor of PSA. The only other compound with similar activity was **10**, with an estimated IC₅₀ of 7.8 μ M. Overall, **11** displayed the strongest dose-dependent inhibition of PSA with an IC₅₀ of approximately 250 nM. From this data, the *p*-carbamoyl moiety is clearly more specific in binding to PSA, as it is believed to be more specific to the P1 site of the enzyme than the *p*-hydroxy group of **4**.

Due to experimental constraints, IC₅₀ values for compounds **2**, **3**, and **5** could not be determined. These compounds lacked the desired solubility for the designed buffer system containing 10% DMSO and concentration range to properly determine dose concentration at 50% PSA activity. As a consequence, extrapolation of a logIC₅₀ value from the dose response curve could not be calculated. Instead, relative enzymatic activities at 250 μ M final concentration are reported.

3.5. Comparison of Docking Scores vs Experimental Values. In order to assess the validity of our computational model, log IC₅₀ values extrapolated from dose-dependent response curves were plotted against docking scores obtained from the AutoDock scoring algorithm. Using the method described, empirical and model results correlated especially well within the bounds established in the protocol, as seen in Figure 7. The comparison of ten compounds and their scores resulted in a $R^2 = 0.732$. Since the enantiomers of the compounds were not separated and tested individually in the kinetic assays, both

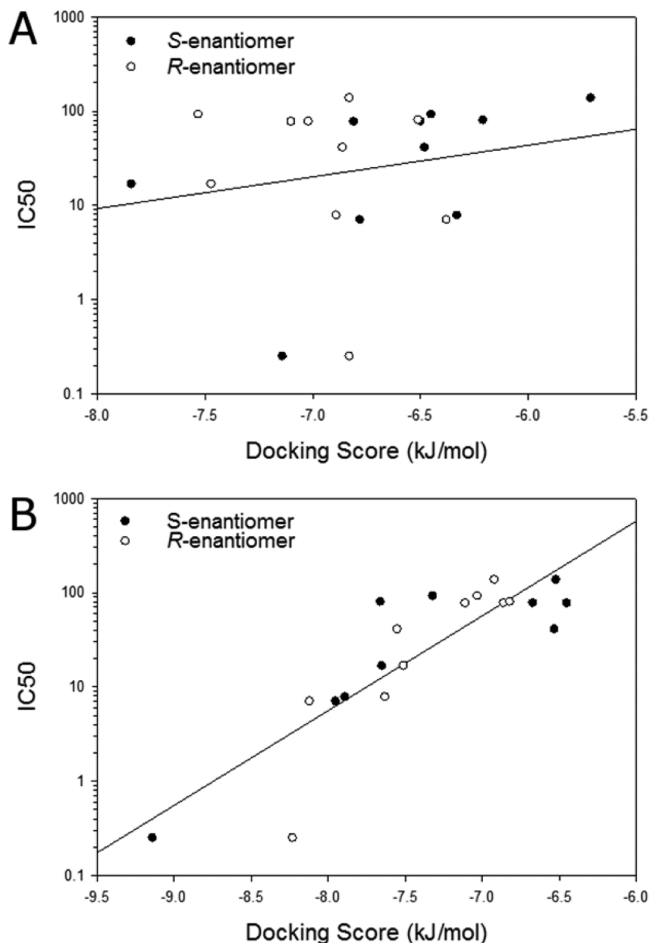


Figure 7. Plot of $\log IC_{50}$ vs docking score obtained from AutoDock molecular docking simulations using (a) a single atom constraint and conventional search protocols and (b) the covalent tether constraint described in this paper.

R- and S-enantiomer scores of a compound were plotted vs identical $\log IC_{50}$ values. Compounds 2, 3, and 5 were omitted from the plot since IC_{50} values could not be determined due to the limits of the experiment.

The results were compared to the more naïve method of molecular docking, utilizing a global search with a single atom constraint on the phosphorus atom of the inhibitor to the hydroxyl functional group of SER₁₉₅. The comparison in both instances yielded no appreciable match in trend between the model and the experimental data ($R^2 = 0.042$). This can be explained by the size of the search space within the binding site of the protein. With significant volume size in a site of interest, false positives become more visible due to the expanded conformational degrees of freedom of the ligand. As a consequence, improper poses not analogous to crystallographic data are incorrectly scored.²⁵ This is commonly described as the Achilles' heel of molecular docking experiments, since limiting the number of false positives in high-throughput screening has been problematic.

Overall, the docking energies using the single-atom constraint scored lower than the covalent tether method. The penalty that arises from steric clashes with neighboring atoms in proximity to the Gaussian well factor into the lower scores obtained. The lack of parameter settings in the AutoDock suite hinders the accuracy of this method.⁴⁸ Traditional methods

failed to provide a top pose that resembled crystallographic structures obtained from homology models without imposing some selection bias. The flexible side-chain approach was able to circumvent these issues. As a result, the expanded flexible side-chain methodology described in this paper has shown to be a more suitable choice as a predictor of drug potency.

4. CONCLUSION

We have described an effective method for the development of novel PSA inhibitors using a convenient synthetic route to yield diphenyl α -aminoalkylphosphonates. Using the molecular docking software AutoDock, we optimized binding at the S1 position of the substrate. The modeling methodology employed demonstrated a significant correlation between in silico ligand binding energies to in vitro dose-dependent inhibition values. From the modeling, it is thought that the push–pull hydrogen bonding arrangement between S1/P1 functionalities are responsible for favorable docking scores, specifically the interactions between the P1 residues of THR₁₉₀, SER₂₁₇, and SER₂₂₇ and the carbamoyl group of the inhibitor. Through MD simulations via GROMACS, these interactions were consistent throughout the 5 ns simulation without major fluctuations of the ligand within the binding cavity.

Although there was some success in correlating molecular docking studies to biological evaluation of diphenyl α -aminoalkylphosphonates, it was not without some errors. The IC_{50} of 5 was far more potent than what was predicted from the molecular docking studies. The more likely reason for this may lie with assignment of partial charges in the AutoDock suite, thus leading to improperly scoring a polar interaction between P1 residues with the cyano moiety. Atom type assignments in AutoDock can be adjusted to better characterize the aryl-cyano group topology and resolve issues regarding false positives. As with any de novo drug design, ligand topologies must sometimes be modified to determine more probable charge distributions.

The work presented here can be expanded tremendously to optimize PSA inhibition and develop enzyme-selectivity. We propose that the benzyl carbamate protecting group within our synthesized compounds can be supplanted with various small molecules or amino acids via amide coupling reactions to probe the selectivity and potency from our lead compound. The success of our S1 and P1 docking-directed generation of the inhibitors paves the way to our future work utilizing ligand docking experiments to optimize S2 and S3 positions to create di- and tripeptide mimics of PSA by screening a small virtual library of compounds. This library can be searched via high-throughput virtual screening to score the tripeptide ligands against other proteases to optimize selectivity toward PSA and circumvent drug promiscuity.

ASSOCIATED CONTENT

S Supporting Information

- Structure alignment between PSA and trypsin as well as their corresponding ligands (Figure S1).
 - Ligand topology file, including atom type and partial charges, for compound S11 in MD studies (Table S1).
 - Charges assigned to PSA receptor residues in MD simulations (Table S2).
- This material is available free of charge via the Internet at <http://pubs.acs.org>.

AUTHOR INFORMATION

Corresponding Author

*Tel.: 01-215-895-2562. Fax: 01-215-895-1265. E-mail: hj56@drexel.edu.

Notes

The authors declare no competing financial interest.

ACKNOWLEDGMENTS

We would like to thank Dr. Justin Lemkul for assisting in MD simulations presented in this paper. C.Y. thanks a grant from NCI of National Institutes of Health, NCI-NIH 1R15CA089162-01.

ABBREVIATIONS

PSA, prostate-specific antigen; PCa, prostate cancer; TGF-P/ β , transforming growth factor type P/beta; KLK3, kallikrein-related peptidase-3; IGF-I/II, insulin-like growth factor type I/II; IGFBP-3, insulin-like growth factor binding protein type 3; VS, virtual screen; MD, molecular dynamics; PME, Particle Mesh Ewald; NMR, nuclear magnetic resonance; HRMS, high-resolution mass spectrometry; CI, chemical ionization; DMSO, dimethyl sulfoxide; 4PL, 4-point log; LGA, Lamarckian genetic algorithm; VMD, visual molecular dynamics; RMSD, root-mean squared deviation; RMSF, root-mean squared fluctuation; CKL, classic kallikrein loop; IC₅₀, half-maximal inhibitory concentration

REFERENCES

- (1) American Cancer Society. *Cancer Facts & Figures* 2014; Atlanta, 2014; pp 1–72.
- (2) Roddam, A. W.; Duffy, M. J.; Hamdy, F. C.; Ward, A. M.; Patnick, J.; Price, C. P.; Rimmer, J.; Sturgeon, C.; White, P.; Allen, N. E. Use of Prostate-Specific Antigen (PSA) Isoforms for the Detection of Prostate Cancer in Men with a PSA Level of 2–10 Ng/mL: Systematic Review and Meta-Analysis. *Eur. Urol.* **2005**, *48*, 386–399.
- (3) Diamandis, E. P. Prostate-Specific Antigen: Its Usefulness in Clinical Medicine. *Trends Endocrinol. Metab.* **1998**, *9*, 310–316.
- (4) Lilja, H.; Oldbring, J.; Rannevik, G.; Laurell, C. B. Seminal Vesicle-Secreted Proteins and Their Reactions during Gelation and Liquefaction of Human Semen. *J. Clin. Invest.* **1987**, *80*, 281–285.
- (5) Kim, J.; Coetzee, G. A. Prostate Specific Antigen Gene Regulation by Androgen Receptor. *J. Cell. Biochem.* **2004**, *93*, 233–241.
- (6) Rowlands, M.-A.; Holly, J. M. P.; Gunnell, D.; Donovan, J.; Lane, J. A.; Hamdy, F.; Neal, D. E.; Oliver, S.; Smith, G. D.; Martin, R. M. Circulating Insulin-like Growth Factors and IGF-Binding Proteins in PSA-Detected Prostate Cancer: The Large Case-Control Study ProtecT. *Cancer Res.* **2012**, *72*, 503–515.
- (7) Killian, C. S.; Corral, D. A.; Kawinski, E.; Constantine, R. I. Mitogenic Response of Osteoblast Cells to Prostate-Specific Antigen Suggests an Activation of Latent TGF-Beta and a Proteolytic Modulation of Cell Adhesion Receptors. *Biochem. Biophys. Res. Commun.* **1993**, *192*, 940–947.
- (8) Maeda, H.; Yonou, H.; Yano, K.; Ishii, G.; Saito, S.; Ochiai, A. Prostate-Specific Antigen Enhances Bioavailability of Insulin-like Growth Factor by Degrading Insulin-like Growth Factor Binding Protein 5. *Biochem. Biophys. Res. Commun.* **2009**, *381*, 311–316.
- (9) Harris, W. P.; Mostaghel, E. A.; Nelson, P. S.; Montgomery, B. Androgen Deprivation Therapy: Progress in Understanding Mechanisms of Resistance and Optimizing Androgen Depletion. *Nat. Clin. Pract. Urol.* **2009**, *6*, 76–85.
- (10) Karantanos, T.; Corn, P. G.; Thompson, T. C. Prostate Cancer Progression after Androgen Deprivation Therapy: Mechanisms of Castrate Resistance and Novel Therapeutic Approaches. *Oncogene* **2013**, *32*, 5501–5511.
- (11) Yang, C. F.; Porter, E. S.; Boths, J.; Kanyi, D.; Hsieh, M.-C.; Cooperman, B. S. Design of Synthetic Hexapeptide Substrates for Prostate-Specific Antigen Using Single-Position Minilibraries. *J. Pept. Res.* **1999**, *54*, 444–448.
- (12) LeBeau, A. M.; Singh, P.; Isaacs, J. T.; Denmeade, S. R. Potent and Selective Peptidyl Boronic Acid Inhibitors of the Serine Protease Prostate-Specific Antigen. *Chem. Biol.* **2008**, *15*, 665–674.
- (13) Singh, P.; Williams, S. A.; Shah, M. H.; Lectka, T.; Pritchard, G. J.; Isaacs, J. T.; Denmeade, S. R. Mechanistic Insights into the Inhibition of Prostate Specific Antigen by Beta-Lactam Class Compounds. *Proteins* **2008**, *70*, 1416–1428.
- (14) Oleksyszyn, J.; Tyka, R. An Improved Synthesis of 1-Aminophosphonic Acids. *Tetrahedron Lett.* **1977**, *18*, 2823–2824.
- (15) Fields, E. K. The Synthesis of Esters of Substituted Amino Phosphonic Acids. *J. Am. Chem. Soc.* **1952**, *74*, 1528–1531.
- (16) Kabachnik, M. I.; Medved, T. I. [New Method of Synthesis of Alpha-Aminoalkylphosphinic Acids]. *Izv. Akad. Nauk SSSR. Otdelenie Khim. Nauk* **1953**, *5*, 868–878.
- (17) Oleksyszyn, J.; Boduszek, B.; Kam, C. M.; Powers, J. C. Novel Amidine-Containing Peptidyl Phosphonates as Irreversible Inhibitors for Blood Coagulation and Related Serine Proteases. *J. Med. Chem.* **1994**, *37*, 226–231.
- (18) Bertrand, J. A.; Oleksyszyn, J.; Kam, C. M.; Boduszek, B.; Presnell, S.; Plaskon, R. R.; Suddath, F. L.; Powers, J. C.; Williams, L. D. Inhibition of Trypsin and Thrombin by amino(4-Amidinophenyl)-methanephosphonate Diphenyl Ester Derivatives: X-Ray Structures and Molecular Models. *Biochemistry* **1996**, *35*, 3147–3155.
- (19) Sieńczyk, M.; Oleksyszyn, J. Inhibition of Trypsin and Urokinase by Cbz-amino(4-Guanidinophenyl)methanephosphonate Aromatic Ester Derivatives: The Influence of the Ester Group on Their Biological Activity. *Bioorg. Med. Chem. Lett.* **2006**, *16*, 2886–2890.
- (20) Schultz, C.; Aime, S.; Sieńczyk, M.; Podgórski, D.; Błażejewska, A.; Kulbacka, J.; Saczko, J.; Oleksyszyn, J. Phosphonic Pseudopeptides as Human Neutrophil Elastase Inhibitors—a Combinatorial Approach. *Bioorg. Med. Chem.* **2011**, *19*, 1277–1284.
- (21) Yang, C. F.; Zakreski, R.; Li, W.; Mou, X.; Iltchenko, N.; Cooperman, B. S. Proteolytic Inhibition in Regulating the Insulin-Like Growth Factor-Binding Proteins in Prostate Cancer. *Biochem. Physiol. Open Access* **2012**, *1*, 1–8.
- (22) Ménez, R.; Michel, S.; Muller, B. H.; Bossus, M.; Ducancel, F.; Jolivet-Reynaud, C.; Stura, E. a. Crystal Structure of a Ternary Complex between Human Prostate-Specific Antigen, Its Substrate Acyl Intermediate and an Activating Antibody. *J. Mol. Biol.* **2008**, *376*, 1021–1033.
- (23) Morris, G. M.; Goodsell, D. S.; Halliday, R. S.; Huey, R.; Hart, W. E.; Belew, R. K.; Olson, A. J. Automated Docking Using a Lamarckian Genetic Algorithm and an Empirical Binding Free Energy Function. *J. Comput. Chem.* **1998**, *19*, 1639–1662.
- (24) Huey, R.; Morris, G. M.; Olson, A. J.; Goodsell, D. S. A Semiempirical Free Energy Force Field with Charge-Based Desolvation. *J. Comput. Chem.* **2007**, *28*, 1145.
- (25) Morris, G. M.; Huey, R.; Lindstrom, W.; Sanner, M. F.; Belew, R. K.; Goodsell, D. S.; Olson, A. J. AutoDock4 and AutoDockTools4: Automated Docking with Selective Receptor Flexibility. *J. Comput. Chem.* **2009**, *30*, 2785–2791.
- (26) Jackson, D. S.; Fraser, S. a.; Ni, L. M.; Kam, C. M.; Winkler, U.; Johnson, D. a.; Froelich, C. J.; Hudig, D.; Powers, J. C. Synthesis and Evaluation of Diphenyl Phosphonate Esters as Inhibitors of the Trypsin-like Granzymes A and K and Mast Cell Tryptase. *J. Med. Chem.* **1998**, *41*, 2289–2301.
- (27) Pronk, S.; Páll, S.; Schulz, R.; Larsson, P.; Bjelkmar, P.; Apostolov, R.; Shirts, M. R.; Smith, J. C.; Kasson, P. M.; van der Spoel, D.; Hess, B.; Lindahl, E. GROMACS 4.5: A High-Throughput and Highly Parallel Open Source Molecular Simulation Toolkit. *Bioinformatics* **2013**, *29*, 845–854.
- (28) Hornak, V.; Abel, R.; Okur, A.; Strockbine, B.; Roitberg, A.; Simmerling, C. Comparison of Multiple Amber Force Fields and

- Development of Improved Protein Backbone Parameters. *Proteins* **2006**, *65*, 712–725.
- (29) Wang, J.; Wang, W.; Kollman, P. A.; Case, D. A. Automatic Atom Type and Bond Type Perception in Molecular Mechanical Calculations. *J. Mol. Graph. Model.* **2006**, *25*, 247–260.
- (30) Wang, J.; Wolf, R. M.; Caldwell, J. W.; Kollman, P. A.; Case, D. A. Development and Testing of a General Amber Force Field. *J. Comput. Chem.* **2004**, *25*, 1157–1174.
- (31) Sousa da Silva, A. W.; Vranken, W. F. ACPYPE - AnteChamber PYthon Parser interface. *BMC Res. Notes* **2012**, *5*, 367–374.
- (32) Solmajer, A. P. U. B. T. Binding Free Energy Calculations of N-Sulphonyl-Glutamic Acid Inhibitors of MurD Ligase. *J. Mol. Model.* **2009**, *15*, 983–996.
- (33) Ectors, P.; Duchstein, P.; Zahn, D. Nucleation Mechanisms of a Polymorphic Molecular Crystal: Solvent-Dependent Structural Evolution of Benzamide Aggregates. *Cryst. Growth Des.* **2014**, *14*, 2972–2976.
- (34) Jorgensen, W. L.; Chandrasekhar, J.; Madura, J. D.; Impey, R. W.; Klein, M. L. Comparison of Simple Potential Functions for Simulating Liquid Water. *J. Chem. Phys.* **1983**, *79*, 926–935.
- (35) Pullman, B., Ed. *Intermolecular Forces*; D. Reidel Publishing Company: Dordrecht, 1981; pp 331–342.
- (36) Darden, T.; York, D.; Pedersen, L. Particle Mesh Ewald: An N Log (N) Method for Ewald Sums in Large Systems. *J. Chem. Phys.* **1993**, *98*, 10089–10092.
- (37) Verlet, L. Computer “Experiments” on Classical Fluids. I. Thermodynamical Properties of Lennard-Jones Molecules. *Phys. Rev.* **1967**, *159*, 98–103.
- (38) Bussi, G.; Donadio, D.; Parrinello, M. Canonical Sampling through Velocity Rescaling. *J. Chem. Phys.* **2007**, *126*, 014101.
- (39) Parrinello, M. Polymorphic Transitions in Single Crystals: A New Molecular Dynamics Method. *J. Appl. Phys.* **1981**, *52*, 7182–7190.
- (40) Humphrey, W.; Dalke, A.; Schulten, K. VMD: Visual Molecular Dynamics. *J. Mol. Graph.* **1996**, *14*, 33–38.
- (41) Moreau, T.; Gauthier, F. Homology Modelling of Rat Kallikrein rK9, a Member of the Tissue Kallikrein Family: Implications for Substrate Specificity and Inhibitor Binding. *Protein Eng.* **1996**, *9*, 987–995.
- (42) Oleksyszyn, J.; Subotkowska, L.; Mastalerz, P. Diphenyl 1-Aminoalkanephosphonates. *Synthesis (Stuttg.)* **1979**, *1979*, 985–986.
- (43) Oleksyszyn, J.; Subotkowska, L. Aminomethanephosphonic Acid and Its Diphenyl Ester. *Synthesis (Stuttg.)* **1980**, *1980*, 906–906.
- (44) Oleksyszyn, J. 1-N-Alkylaminoalkanephosphonic and 1-N-Alkylaminoalkylphenylphosphinic Acids. *Synthesis (Stuttg.)* **1980**, *1980*, 722–724.
- (45) Bhagat, S.; Chakraborti, A. K. An Extremely Efficient Three-Component Reaction of Aldehydes/ketones, Amines, and Phosphites (Kabachnik-Fields Reaction) for the Synthesis of Alpha-Amino-phosphonates Catalyzed by Magnesium Perchlorate. *J. Org. Chem.* **2007**, *72*, 1263–1270.
- (46) Weigert, F. J.; Roberts, J. D. Nuclear Magnetic Resonance Spectroscopy. Spin-Spin Coupling of Carbon to Phosphorus, Mercury, Nitrogen, and Other Elements. *Inorg. Chem.* **1973**, *12*, 313–316.
- (47) Joossens, J.; Van der Veken, P.; Surpateanu, G.; Lambeir, A.-M.; El-Sayed, I.; Ali, O. M.; Augustyns, K.; Haemers, A. Diphenyl Phosphonate Inhibitors for the Urokinase-Type Plasminogen Activator: Optimization of the P4 Position. *J. Med. Chem.* **2006**, *49*, 5785–5793.
- (48) Ouyang, X.; Zhou, S.; Su, C. T. T.; Ge, Z.; Li, R.; Kwok, C. K. CovalentDock: Automated Covalent Docking with Parameterized Covalent Linkage Energy Estimation and Molecular Geometry Constraints. *J. Comput. Chem.* **2013**, *34*, 326–336.